Effect of Ser392 Phosphorylation on the Structure and Dynamics of the Polybasic Domain of ADP Ribosylation Factor Nucleotide Site Opener Protein: A Molecular Simulation Study

Kannan Srinivasaraghavan,*[,†,‡] Kassoum Nacro,[‡] Gerhard Grüber,[†,§] and Chandra S. Verma*[,†,§,‖]

[†]Bioinformatics Institute (A*STAR), 30 Biopolis Street, 07-01 Matrix, Singapore 138671
[‡]Experimental Therapeutics Centre (A*STAR), 31 Biopolis Street, 03-01 Nanos, Singapore 138669
[§]School of Biological Sciences, Nanyang Technological University, 60 Nanyang Drive, Singapore 637551
[‖]Department of Biological Sciences, National University of Singapore, 14 Science Drive 4, Singapore 117543

Ⓢ *Supporting Information*

ABSTRACT: ADP ribosylation factor nucleotide site opener (ARNO) as a guanine nucleotide exchange factor (GEF) activates small GTPases called ADP ribosylation factors (Arfs), which function as molecular switches and regulate a variety of cell biological events. ARNO directly interacts with the transmembrane a2-subunit isoform of the proton-pumping vacuolar ATPase in an acidification-dependent manner, and this interaction plays a crucial role in the regulation of the protein degradation pathway. A recent study reported specific interactions of a2N with the $ARNO_{375-400}$ peptide correspond-

ing to the polybasic (PB) domain of ARNO, which is a crucial regulatory element in the autoregulation and modulation of Arf-GEF activity. Interestingly, phosphorylation of Ser392 completely abolishes this interaction, and the experimental structure shows significant structural rearrangements. To investigate the effect of Ser392 phosphorylation on the structure and dynamics of the $ARNO_{375-400}$ peptide, we employed all atom molecular dynamics (MD) simulations of the phosphorylated and unphosphorylated PB domain of the ARNO protein. A Hamiltonian-based replica exchange method called biasing potential replica exchange MD was used to enhance conformational sampling. Simulations predicted that the isolated PB domain is highly flexible, with the C-terminal region of the unphosphorylated state being unstable. In contrast, Ser392 phosphorylation increases the overall stability of the peptide. In agreement with experimental results, our simulations further support the hypothesis that phosphorylation induces disorder to order transitions and provide new insights into the structural dynamics of the PB domain. Phosphorylation of Ser392 appears to stabilize the C-terminal α-helix via formation of salt bridges between phospho-Ser392 and Arg390, Lys395, and Lys396.
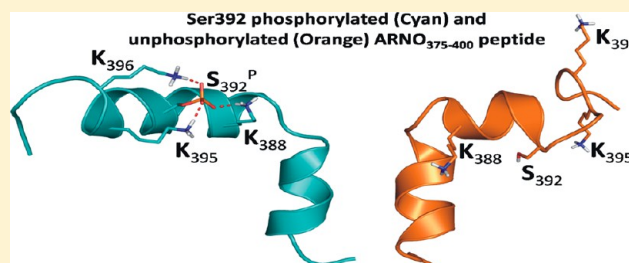
ARNO (ADP ribosylation factor nucleotide site opener), also known as cytohesin-2, is a member of the cytohesin subfamily, which also includes cytohesin-1, cytohesin-3, and cytohesin-4.[1] These four human isoforms are closely related and share a common sequence (~80% similar sequences) and structural domain organization. The latter consists of an N-terminal coiled-coil (CC) domain and a central Sec7 domain in tandem with a phosphoinositide-binding pleckstrin homology (PH) domain and a short C-terminal polybasic (PB) domain that is rich in positively charged amino acids. ARNO as a guanine nucleotide exchange factor (GEF) activates small GTPases called ADP ribosylation factors (Arfs), which function as molecular switches and regulate a variety of cell biological events.[2−4] The ADP ribosylation factors (Arfs) belong to a family of small, ubiquitously expressed and evolutionarily conserved guanosine triphosphatases that play a key regulatory role in vesicular transport in eukaryotic cells. Both ARNO and Arfs, especially Arf6, have been implicated in endocytosis by regulating actin cytoskeleton remodeling, lipid modifications

and rearrangements, and carrier vesicle coat formation.[5,6] It has been demonstrated that ARNO, along with Arf6, is recruited from the cytosol to the endosomal membranes in an acidification-dependent manner by a proton pumping vacuolar ATPase (V-ATPase).[5−7] In particular, it was shown that the transmembrane a2-subunit isoform of the V-ATPase directly interacts with ARNO and this interaction plays a crucial role in the regulation of the protein degradation pathway.[5−7] Recent pull-down experiments suggested that this is a complex multisite interaction and identified a specific, direct interaction of a2N with the $ARNO_{375-400}$ peptide corresponding to the PB domain of ARNO.[8] The PB domain of the cytohesin family is a crucial regulatory element in the autoregulation and modulation of their Arf-GEF activity.[9] Interestingly, phosphorylation of Ser392 completely abolishes the interaction of the PB

domain of the ARNO protein with the a2N peptide. Three-dimensional nuclear magnetic resonance (NMR) structures of the isolated PB domain of ARNO show significant structural rearrangements resulting from Ser392 phosphorylation.[8] While both the phosphorylated and unphosphorylated forms of the isolated PB domain of ARNO form stable α-helices at the N-terminus (Figure 1), significant structural changes were
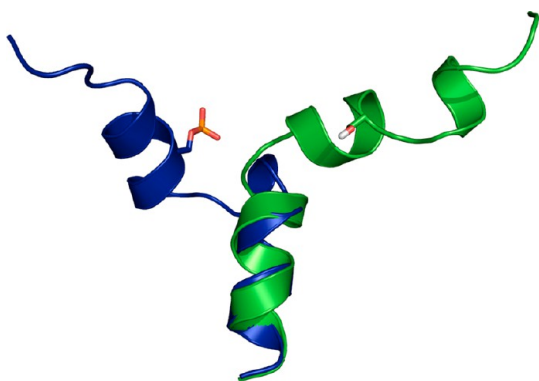

Figure 1. Cartoon representation of superimposition via N-terminal residues (375−385) of the average structure of (blue) phosphorylated ARNO$_{375-400}^{P}$ and (green) unphosphorylated ARNO$_{375-400}$ showing the phosphorylation-dependent conformational changes between the C-terminal helices. Ser392 and phospho-Ser392 are highlighted as sticks.

observed for the C-terminal regions. The phosphorylated form of the peptide forms a stable helix−loop−helix structure with an α-helix at the N- and C-termini. The unphosphorylated peptide forms a stable short helix at the N-terminal helix with a very unstable and highly flexible 3_{10}-helix at the C-terminus. Thus, Ser392 phosphorylation of the ARNO$_{375-400}^{P}$ peptide appears to be associated with significant structural changes at the C-terminus, resulting in the disruption of the α-helical motif at Ser392 in unphosphorylated ARNO$_{375-400}$.

Phosphorylation-associated modulation and regulation have been studied extensively using experimental and simulation methods and have exhibited both ordering and disordering effects of phosphorylation in different proteins and peptides. Employing Monte Carlo/stochastic dynamics on a polyalanine peptide capped with phosphoserine at the N-terminus, Smart and McCammon reported that phosphorylation stabilizes the helix via simple electrostatic interactions.[10] Recent experimental and computational studies of the isolated phosphorylation domain of smooth muscle myosin also predicted a disorder-to-order transition induced by phosphorylation of Ser19 in the 25-residue α-helix at the N-terminus.[11,12] Magnetic resonance experiments[13,14] and molecular dynamics (MD) simulations[15] demonstrated that destabilization of an α-helix at the N-terminus of the phospholamban (PLB) protein is induced by phosphorylation of Ser16 in its cytoplasmic domain. Experimental studies of a 19-residue helical peptide of stathmin (55−73) have indicated that phosphorylation of Ser63 destabilizes the helical structure and as a consequence the tublin binding properties of stathmin.[16] This appears to result from disruption of salt bridges that stabilize the helical structure, as shown by recent MD simulation studies.[17]

It is known that in the ARNO protein, phosphorylation of PB domain Ser392 by protein kinase C (PKC) regulates its Arf-GEF activity.[18] However, the molecular mechanism of this regulation remains undetermined. To explore the effect of the

phosphorylation of Ser392, we employ all atom MD simulations on the isolated PB domain of the ARNO protein. In addition to standard MD simulations, an advanced sampling method has also been used to explore the effects of Ser392 phosphorylation on the structure and dynamics of the ARNO PB domain. Recently, a developed Hamiltonian-based replica exchange method, called biasing potential replica exchange MD (BP-REMD),[19] has been used to enhance the conformational sampling of the ARNO peptides during the MD simulations. This method focuses on the protein backbone flexibility and employs a specific biasing potential to promote peptide backbone transitions as a replica coordinate. The biasing potential lowers the barriers associated with peptide backbone dihedral transitions. The level of biasing is gradually changed along the replicas such that frequent transitions are possible at high levels of biasing and the system can escape from becoming trapped in local energy minima. Because exchanges between replicas are independent of the number of solvent molecules, the method requires many fewer replicas for efficient sampling compared with methods such as standard temperature REMD.[19,20] The method has been extensively benchmarked on several systems and has demonstrated significantly improved conformational sampling compared with that of standard MD simulations.[21−23]

■ MATERIALS AND METHODS

The experimental structure of both phosphorylated [Protein Data Bank (PDB) entry 2kpa] and unphosphorylated (PDB entry 2kpb) forms of the isolated PB domain of ARNO protein was used as the starting structure for MD simulations. Hydrogen atoms were added to the experimental structures using the Xleap module of the Amber11 package.[24] Both systems were neutralized by the addition of counterions. The neutralized system was solvated with TIP3P[25] water molecules to form a truncated octahedral box with at least 10 Å separating the solute atoms and the edges of the box. MD simulations were conducted with the Sander module of the Amber11 package in combination with the parm03 force field.[26] Force field parameters for phosphorylated serine were taken as described elsewhere.[27] For the phosphate groups, an overall charge of −2e has been used.

All the systems were first subjected to 100 steps of energy minimization. This was followed by MD simulations, for which the protein was initially harmonically restrained (25 kcal mol^{-1} Å^2) to the energy-minimized coordinates, and the system was heated to 300 K in steps of 100 K followed by the gradual removal of the positional restraints and a 1 ns unrestrained equilibration at 300 K. The resulting system was used for both the BP-REMD and conventional MD simulations.

The BP-REMD method is a Hamiltonian REMD method that employs a biasing potential for the Φ and Ψ peptide backbone dihedral angles.[19] The biasing potential is based on a potential of mean force (PMF) for each of the two dihedral angles calculated for a model peptide (alanine dipeptide) in explicit solvent. Addition of the biasing potential during a simulation lowers the energy barriers for backbone dihedral transitions in a peptide or protein, resulting in increased flexibility in the protein chain. During BP-REMD, the level of biasing is gradually changed along the replicas such that frequent transitions are possible at high levels of biasing. The same biasing potential derived from the model system was used for all backbone dihedrals in the protein. In a BP-REMD simulation, different biasing potential levels are applied in each

replica (one reference replica run is conducted without any biasing potential) and replica exchanges between neighboring biasing levels were attempted every 1000 MD steps and accepted or rejected according to a Metropolis criterion.[28]

For each case, five independent (using different initial random velocities) MD simulations and a biasing potential replica exchange MD simulation with five replicas were conducted starting from the well-equilibrated experimental structure. Each MD simulation was conducted for 200 ns, and conformations were recorded every 10 ps. BP-REMD simulations were conducted for 25 ns, and exchanges between neighboring biasing levels were attempted every 2 ps, thus resulting in 12500 attempted exchanges with an acceptance probability for replica exchange in the range of ~35%.

We also conducted a simulation starting from the experimental conformation of phosphorylated $ARNO_{375-400}$ peptide but with Ser392 dephosphorylated. This was conducted by replacing the phosphate group with a hydrogen atom and was done to investigate robustness associated with the phosphorylation-dependent induction of disorder from the ordered C-terminus of the $ARNO_{375-400}$ peptide.

To further examine the dynamics in the context of the full length ARNO protein (without the N-terminal CC region), whose experimental structure is not available, we generated a homology model using Modeller9v2.[29] The crystal structure of ARNO-3 or cytothesin-3 (PDB entry 2r09)[30] in its auto-inhibited form was used as the template. The sequence of the ARNO-2 isoform is 84% identical with that of template ARNO-3. The NMR structure of unphosphorylated and phosphorylated $ARNO_{375-400}$ peptide was used for modeling the unphosphorylated and phosphorylated PB domain. The full length ARNO protein with its PB domain in phosphorylated and unphosphorylated forms was then subjected to MD simulations for 200 ns each.

All MD simulations were conducted in explicit solvent at 300 K. During all the simulations, the long-range electrostatic interactions were treated with the particle mesh Ewald[31] method using a real space cutoff distance of 9 Å. The settle[32] algorithm was used to constrain bond vibrations involving hydrogen atoms, which allowed a time step of 2 fs during the simulations.

ANALYSIS

Interproton distances derived from experimental NOE cross-peak intensities were compared with the average interproton distances calculated from the simulated structures using $\langle r^{-6} \rangle^{-1/6}$ averaging. The results are presented as distance bound violations, i.e., as a difference between the distances averaged over the simulation and the corresponding NMR-derived upper distance bounds. For comparison with simulated trajectories, only a set of NOE distances of backbone protons having $(i, i + 2)$, $(i, i + 3)$, and $(i, i + 4)$ connectivity was considered, because these NOEs are important for secondary structure formation. This resulted in 33 and 39 NOE distances for the unphosphorylated and phosphorylated ARNO peptide, respectively. Average chemical shifts for the α-proton of the peptide backbone were calculated for conformations sampled during the simulations of both the unphosphorylated and phosphorylated forms of the ARNO peptide. α-Proton chemical shifts were calculated using SHIFTX2[33] and are reported as a difference between the calculated average chemical shift of the residue and the respective reference

random-coil chemical shift value. Reference random-coil chemical shift values were taken from ref 34.

Cluster analysis of the sampled conformations was performed using the kclust program in MMTSB-tools.[35] Simulation trajectories were visualized using VMD,[36] and figures were generated using Pymol.[37]

RESULTS

Conformational Dynamics of the Isolated PB Domain. The MD simulations show that both the phosphorylated and unphosphorylated forms of the isolated PB domain are highly flexible. During the standard MD simulations, the unphosphorylated states deviate by up to ~9 Å (the $C\alpha$ rmsd was calculated by superimposing all the residues of sampled structures with the experimental structure) (Figure 2A) from
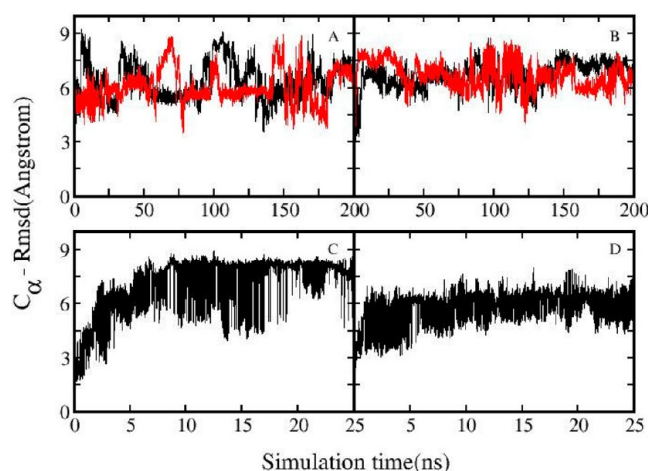

Figure 2. Root-mean-square deviation (rmsd, $C\alpha$) of sampled ARNO peptide conformations in explicit solvent from the native structure vs simulation time. The top panels show continuous MD simulations starting from the experimental structure of (A) unphosphorylated and (B) phosphorylated ARNO peptide (red and black lines correspond to two different sets of initial atomic velocities). The bottom panels show BP-REMD simulations (for the replica run with the original force field) starting from the experimental structure of (C) unphosphorylated and (D) phosphorylated ARNO peptide. The rmsd's were calculated separately by superimposing all the residues of the peptide with the experimental start structure.

the starting state with the conformations undergoing rapid global conformational changes [angle between the helices fluctuates between 75° and 175° (Figure S1 of the Supporting Information)] between ~4 and ~9 Å. While the structural deviations of the phosphorylated states from the starting structure are also quite large, the stability appears to have increased [angle between the helices shows larger fluctuations until ~100 ns, after which the fluctuations are attenuated (Figure S1 of the Supporting Information)], with significant reductions in the temporal fluctuations of the rmsd (Figure 2B and Figure S2 of the Supporting Information). In contrast, during both biasing potential replica exchange MD simulations, frequent transitions between collapsed compact structures and more extended structures were observed (Figure 2C,D). Overall, phosphorylation is associated with an increase in the stability of the $ARNO_{375-400}$ peptide.

Comparison of the NOE distances calculated from the simulated MD trajectories of both phosphorylated and unphosphorylated ARNO peptide shows that the sampled

conformations satisfy all the experimentally determined NOE distance bounds (Figure S3 of the Supporting Information) that are considered here, with minor violations. Most violations do not exceed 1.5 Å and are thus not very significant.

Secondary Structure Fluctuations. Experimentally, it is known that both the phosphorylated and unphosphorylated ARNO-derived peptides form very similar (rmsd ∼ 0.7 Å) and stable α-helices at the N-terminus, but with large structural differences at the C-terminus. In the absence of phosphorylation, the α-helix extending from residue 378 to 384 at the N-terminus is followed by a short loop from residue 385 to 387, a second helix between residues 388 and 391, and a third unstable 3_{10}-helix from residue 394 to 397, with the rest of the C-terminal region being highly flexible. In contrast, the isolated PB domain of the ARNO protein phosphorylated at Ser392 forms a stable helix−loop−helix structure with an N-terminal α-helix extending from residue 377 to 384 and an α-helix at the C-terminus, extending from residue 390 to 396. Alignment of experimental structures at the N-terminus (residues 1−10) reveals a very good overlap in this region (Figure 1) but a deviation of 105° between the C-termini in the loop region. Further comparison of the ensemble of experimental structures highlights the fact that the α-helix in the N-terminal region appears to be relatively stable while the rest of the peptide displays high flexibility; the rmsd ranges between 0.4 and 1.6 Å and between 1.9 and 4.3 Å for the phosphorylated and unphosphorylated states, respectively.

To evaluate the stability of these α-helices at the N- and C-termini of the ARNO-derived peptides, we conducted secondary structure analysis for the conformations that are sampled during MD and BP-REMD simulations. The α-helix at the N-terminus of the unphosphorylated state is stable (>90% of sampled structures) during both the standard MD and BP-REMD simulation, with the rmsd remaining within 2.5 Å (Figure 3A) of the corresponding experimental structure.
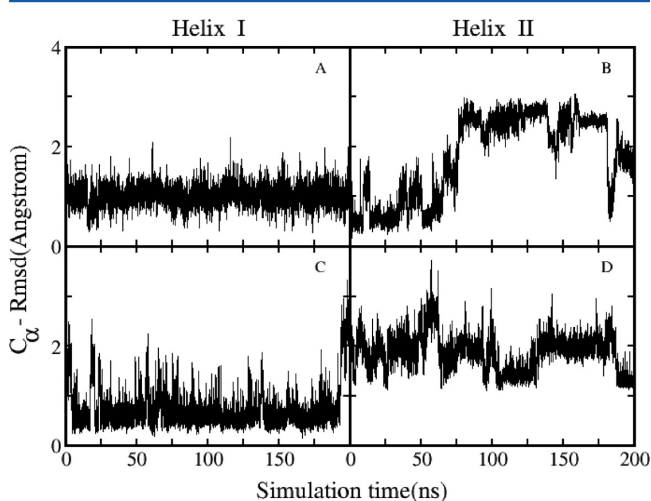

Figure 3. Root-mean-square deviation (rmsd, Cα) of sampled conformations for residues 377−384 (helix I) and 390−396 (helix II) that corresponds to the α-helices at the N- and C-termini of the ARNO peptide, in explicit solvent from the native structure vs simulation time. Continuous MD simulations starting from the experimental structure of (A and B) unphosphorylated and (C and D) phosphorylated ARNO peptide. The rmsd's were calculated separately for helix I and helix II by superimposing only those residues that are part of the α-helices at the N- and C-termini with the experimental start structure.

However, the rest of the peptide is highly flexible (Figures 3B and 4). The second helix at the C-terminus (residues 388−391) was stable for only the first 50 ns, after which it switches to a 3_{10}-helix, and eventually unfolds after ∼100 ns without refolding within the 200 ns time scale of the simulations (Figure 4, top, and Figure S4 of the Supporting Information). The third 3_{10}-helix at the C-terminus of the unphosphorylated peptide is only marginally stable and is not present in most of the sampled conformations (Figure 4, top, and Figure S4 of the Supporting Information). While the BP-REMD simulations capture a much larger conformational landscape, the pattern of high flexibility at the C-terminus, conformational transitions between different conformations, unfolding of the 3_{10}-helix, and general disorder are generally conserved (Figure 4, bottom, and Figure S4 of the Supporting Information).

The phosphorylated peptide fragment of ARNO$_{375−400}$^{P} remains α-helical at the N-terminus during both MD and BP-REMD simulations, with rmsd's remaining within 3.0 Å of the corresponding experimental structure (Figure 3C). In contrast to the unphosphorylated peptide, the second α-helix at the C-terminus of the phosphorylated state is also well-preserved during the simulations (Figures 3D and 4, top, and Figure S4 of the Supporting Information), although conformational transitions between the α-helix and the 3_{10}-helix (Figure 4, bottom) are seen in the BP-REMD simulation. Interestingly, during the BP-REMD simulation, a single overall helix (Figure S5 of the Supporting Information) that spans residues 378−396 was observed very frequently.

The ordering effect associated with phosphorylation is also evident from the analysis of chemical shifts. The secondary proton α (Hα) chemical shift of the phosphorylated ARNO$_{375−400}$^{P} peptide revealed the increased helical content for the entire peptide, except for a few residues at the termini that are flexible (Figure 5B,D). In contrast, in the absence of phosphorylation, helicity was observed for only a portion of the peptide (Figure 5A,C). Thus, the disorder to order transition upon phosphorylation of Ser392 is further supported by the distribution of proton α chemical shifts.

This induction of order upon phosphorylation is consistent with several other studies of a variety of systems.[11,12] In summary, MD simulations predict that the α-helix at the N-terminus of the PB domain of the ARNO-derived peptide is stable, whereas the C-terminus undergoes a disorder to order transition upon phosphorylation.

Conformational cluster analyses based on the pairwise Cartesian (Cα) rmsd between conformations, with an rmsd cutoff of 2 Å, were conducted using the Kclust program in the MMTSB-toolset. BP-REMD of both phosphorylated and unphosphorylated simulations accumulated significantly more distinct conformational states during the simulation time of 25 ns (five replicas with 25 ns each) than the combined five independent classical MD simulations of 200 ns each. This is similar to reports on other peptide and small protein systems.[19−23] The dominant conformational cluster centroids from both simulations of the unphosphorylated states (Figure 6A,B) do have less secondary structure than the phosphorylated states (Figure 6C,D). However, the stable N-terminal α-helix is well preserved in almost all the dominant clusters. Interestingly, during BP-REMD simulations, a single α-helix (Figure 6D), which spans residues 378−396, was observed as the second most populated state of the phosphorylated form of the peptide. In addition, a significant population of conformations (third most highly populated cluster) with an extended α-helix

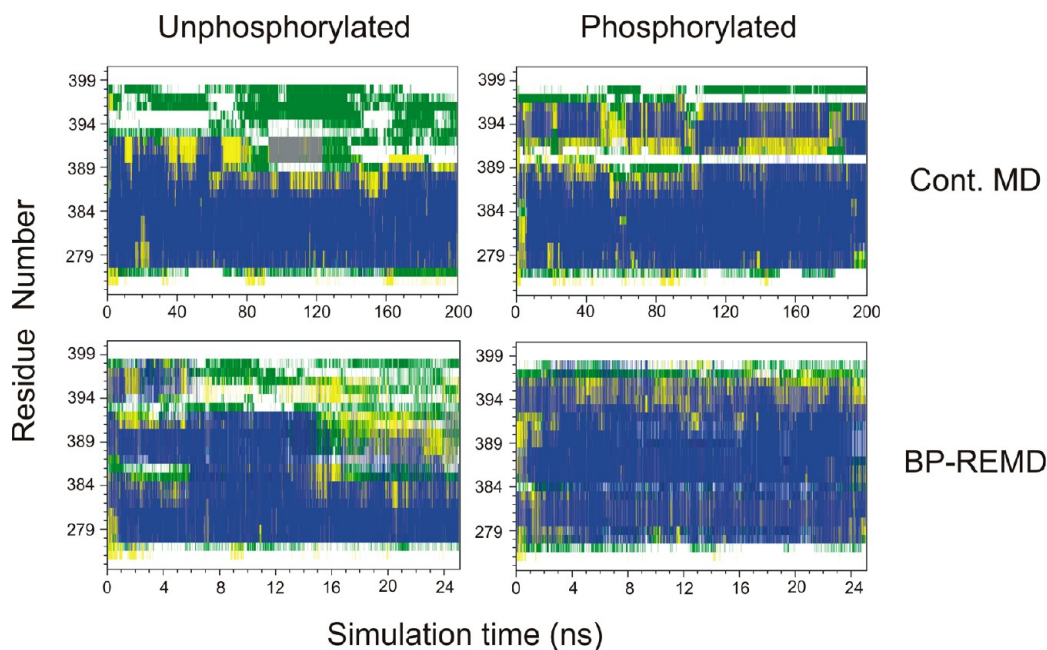Unphosphorylated   Phosphorylated

Figure 4. Evolution of the secondary structure of unphosphorylated (left) and phosphorylated (right) ARNO peptides during cMD (top) and BP-REMD (bottom, for the conformations sampled in the reference replica) simulations. Secondary structure (blue for α-helix, gray for 3_{10}-helix, yellow for turn, green for bend, and white for coil) along the protein chain (y-axis) vs simulation time (x-axis).
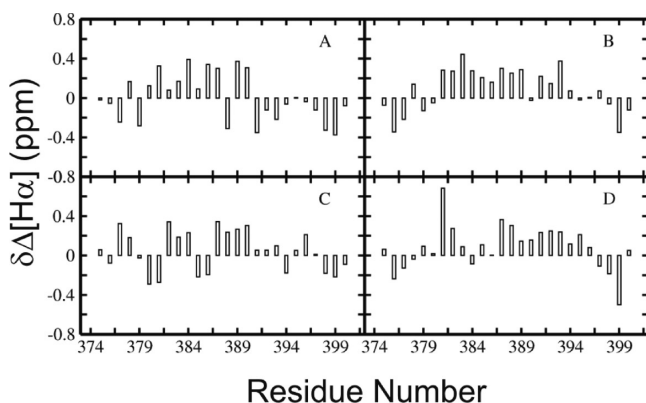

Figure 5. Average secondary proton alpha (Hα) chemical shifts for each residue of the ARNO peptide calculated from the continuous MD simulations of (A) unphosphorylated (B) phosphorylated ARNO peptide and BP-REMD simulations of (C) unphosphorylated and (D) phosphorylated ARNO peptide. +ve and −ve values corresponds to α-helical and β-sheet structures, respectively.

at the N-terminus of the peptide (Figure 6D) was observed during the BP-REMD simulation of the phosphorylated state.

Influence of Ser392 Phosphorylation. As is evident from the NMR structures and MD simulations, important differences in structure and dynamics of the phosphorylated and unphosphorylated fragments were observed. In particular, the C-terminal region of the peptide undergoes the most dramatic changes during the simulations. In the unphosphorylated peptide, this region shows high flexibility and very little secondary structural order. In contrast, the same region in the phosphorylated peptide shows higher structural stability, suggesting that phosphorylation of Ser392 is associated with increased helicity and stability. Detailed analysis of the simulations reveals important interactions that are responsible for this increased helical content, especially in the central region of the PB domain. Phosphorylation of Ser392 preserves the α-helix through a salt bridge or hydrogen bond with the side chains of positively charged residues. Initially, the oxygen atom (OP) of the phosphorylated Ser392 is >10 Å from the amino protons of any positively charged residue (Lys388, Lys389, Arg390, Lys394, and Lys396). However, during both MD and BP-REMD simulations, the side chain of phospho-Ser392 and the side chain of Arg390 come close as the distance between the oxygen of phospho-Ser392 and the Arg390 side chain amino protons decreases to <5 Å, resulting in a salt bridge (Figure 7A,B), which is well preserved during rest of the simulation. In contrast, the corresponding distance [between the side chain oxygen atom (OG) of Ser392 and the Arg390 side chain amino protons] in the unphosphorylated ARNO$_{375-400}$ peptide is >10 Å during most of the simulation (Figure S6 of the Supporting Information). Although a salt bridge was formed [as the distance decreases to <5 Å (Figure S6 of the Supporting Information)] between these two residues, during the early part of the simulation, it is not preserved as the structure unfolds and fluctuates significantly. In addition to the phospho-Ser392−Arg390 interaction, during BP-REMD simulation, a salt bridge or hydrogen bond between phospho-Ser392 and Ly395/Lys396 (Figure 8B) or Lys396/Lys388 (Figure 8C) is also formed and appears to be mainly responsible for stabilizing the emergent helicity of the phosphorylated ARNO$_{375-400}{}^{P}$ peptide. In ~70% of the sampled conformations during BP-REMD, the distance between the oxygen of phospho-Ser392 and amino protons of the Lys396 side chain was <5 Å (Figure 8A), and this interaction was also seen in several small clusters during the normal MD simulations. In summary, the phosphorylation of Ser392 increases both the helical content and the stability of the PB domain of the ARNO-derived peptide through the formation of salt bridges between phospho-Ser392 and Arg390 and/or Lys395/396.

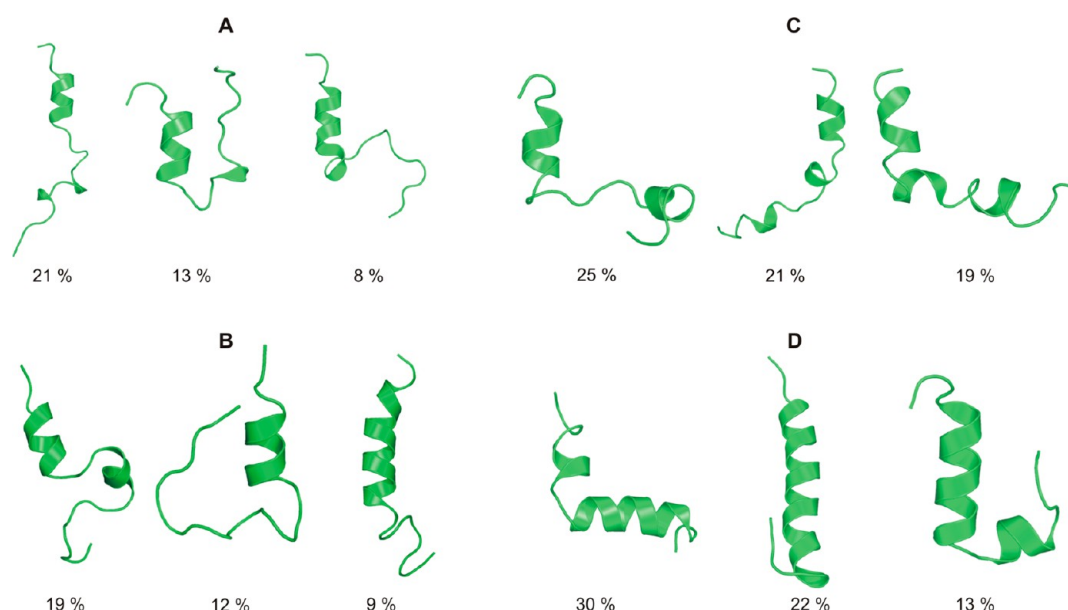Further analysis of the simulations reveals important conformational constraints that are imposed as a result of the

Figure 6. Cartoon representation of cluster centroids (structure closest to the average structure of the cluster) of the three most populated clusters of (A and B) unphosphorylated and (C and D) phosphorylated forms of the peptide during (top, A and C) continuous MD and (bottom, B and D) BP-REMD simulation (in the reference replica), with their corresponding populations shown.
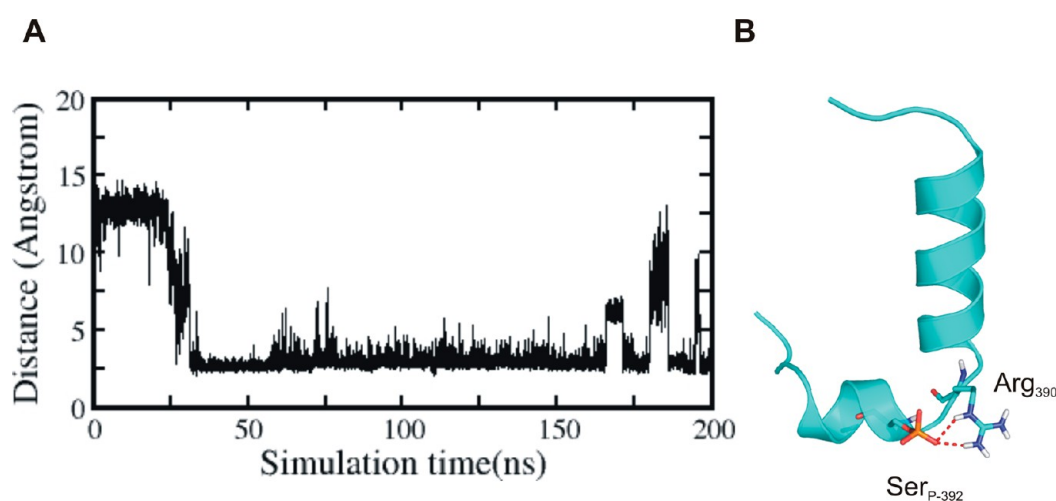

Figure 7. (A) Evolution of the salt bridge during cMD simulation of the phosphorylated $ARNO_{375-400}{}^P$ peptide. Distance between Arg390 side chain amino protons and the phospho-Ser392 oxygen vs simulation time. (B) Structural snapshots illustrating the key residues phospho-Ser392 and Arg390 (stick representation) interacting through a salt bridge or hydrogen bond (red dotted lines).
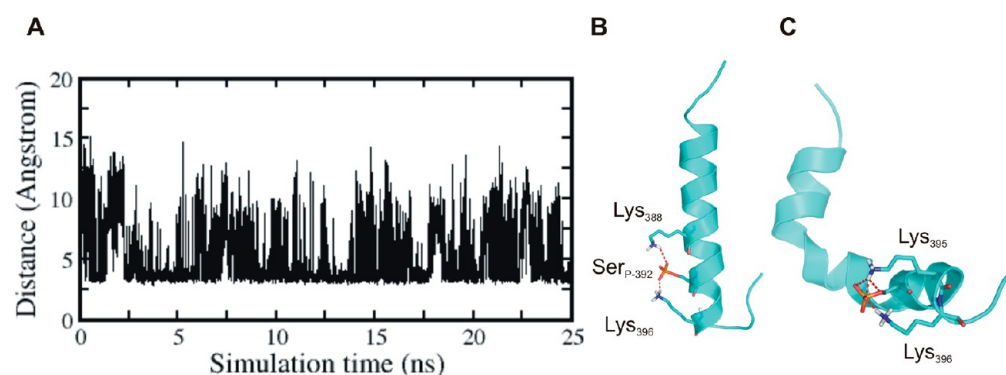

Figure 8. (A) Evolution of the salt bridge during BP-REMD simulation of the phosphorylated $ARNO_{375-400}{}^P$ peptide. Distance between Lys396 side chain amino protons and the phospho-Ser392 oxygen vs simulation time. (B and C) Structural snapshots illustrating the key residues phospho-Ser392 and Lys388, Lys396, and Lys395 (stick representation) interacting through a salt bridge or hydrogen bond (red dotted lines).
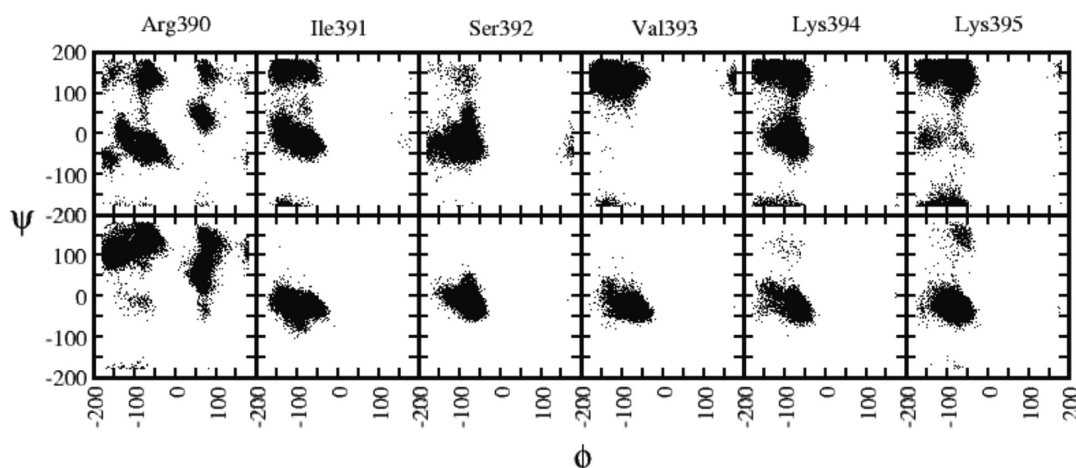
Figure 9. Comparison of backbone dihedral sampling of helix II (residues 390−395) that corresponds to the α-helix at the C-terminus of the ARNO$_{375-400}$^{P} peptide. The top panel in each graph corresponds to the unphosphorylated form of the peptide and the bottom panel to the phosphorylated form.

phosphorylation of Ser392. Formation of stable salt bridge interactions preserves the α-helicity at the C-terminus of the peptide by restricting the backbone conformations of the helical residues. Comparison of the dihedral angles of residues in the sampled conformations of both phosphorylated and unphosporylated simulations reveals restricted conformational flexibility for the residues in the near vicinity of phosphorylated Ser392. The distribution of backbone dihedrals of residues 390−395 shows that the sampling of these residues is mainly restricted to only the α-helical region of the Ramachandran plot, whereas the corresponding residues in the unphosphorylated state are not conformationally restricted (Figure 9) and sample the α-helical and β-sheet regions. In addition, during BP-REMD, the sampled conformations also visit regions of the Ramachandran plot that are specific for extended structures. However, comparison of dihedral angles of residues 378−383 that correspond to the α-helix at the N-terminus of both the phosphorylated and unphosphorylated peptides revealed similar sampling among both states; this is restricted to only the α-helical region of the Ramachandran plot (Figure S7 of the Supporting Information). This restricted backbone flexibility further contributes to the increased stability of the α-helix at the N-terminus (Figure S7 of the Supporting Information).

Interestingly, during both MD and BP-REMD simulations of the phosphorylated state, the stable α-helix at the N-terminus of the ARNO$_{375-400}$ peptide is further extended by an extra turn. This is stabilized by a stable salt bridge interaction between Glu382 and Arg387 (Figure 10B). At the start of the simulation, the distance between Glu382 and Arg387 is >10 Å, which converges to the formation of a salt bridge at ~7.5 ns, as the distance decreases to <5 Å and remains stable (Figure 10A). In addition, during BP-REMD, ~25% of the sampled conformations also show hydrogen bond or salt bridge interactions between the side chains of Glu382 and Lys388 (Figure 10C), which further contributes to the structural stability of the ARNO$_{375-400}$ peptide.

To further investigate (validate) the ordering effect of phospho-Ser392, a 200 ns MD simulation was conducted starting from the phosphorylated conformation of the ARNO$_{375-400}$ peptide, but with Ser392 dephosphorylated. As is evident from the secondary structure analysis of the simulated trajectory, the C-terminal α-helix unfolds at ~40 ns and does not refold within the 200 ns simulation time scale of
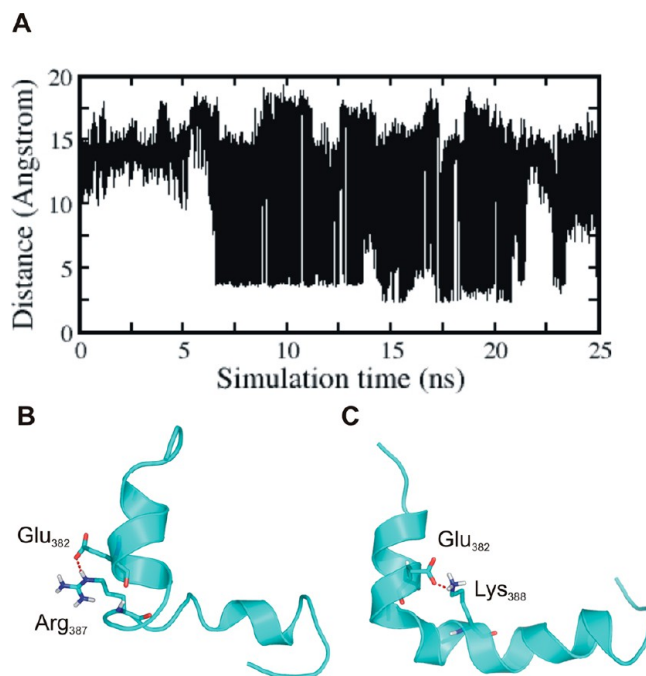

Figure 10. (A) Evolution of the salt bridge during the BP-REMD simulation of the phosphorylated ARNO$_{375-400}$^{P} peptide. Distance between the Glu382 side chain oxygen and the amino protons of the side chain of Arg387 vs simulation time. (B and C) Structural snapshots illustrating the key residues (B) Glu382 and Arg387 and (C) Glu382 and Lys388 (stick representation) interacting through a salt bridge or hydrogen bond (red dotted lines).

the simulation (Figure 11); however, the α-helix at the N-terminus remains relatively stable. This further strengthens the hypothesis that dephosphorylation of Ser392 induces disorder in the C-terminus of the ARNO$_{375-400}$ peptide. Thus, our atomic simulations of the isolated PB domain of the ARNO protein reveal that phosphorylation of Ser392 induces disorder to order transition through stabilization of the α-helix at the C-terminus, an increase in the helicity at the N-terminus, and an increase in the stability of the whole PB domain. This structural ordering upon phosphorylation is emergent and is strengthened by the formation of several stable salt bridges.
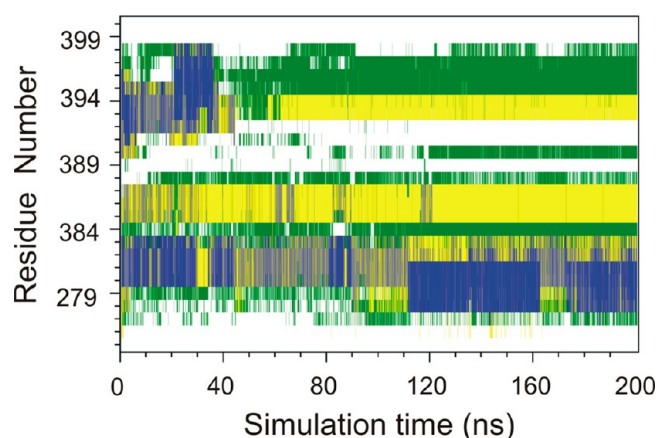
Figure 11. Evolution of the secondary structure of the ARNO$_{375-400}$ peptide starting from the phosphorylated conformation but with dephosphorylated Ser392 during the continuous MD simulations. Secondary structure (blue for α-helix, gray for 3_{10}-helix, yellow for turn, green for bend, and white for coil) along the protein chain (y-axis) vs simulation time (x-axis).

Phosphorylation Induced Conformational Changes in the Full Length ARNO Model Protein. The three-dimensional structure of the complete human ARNO protein without the N-terminal CC region was constructed using the crystal structure of the autoinhibited form of Grp1 (also called ARNO3 or cytothesin-3; PDB entry 2r09) as a template. Guided by the NMR structure of both phosphorylated and unphosphorylated forms of the isolated PB domain, we modeled the full length ARNO protein in the phosphorylated and unphosphorylated forms. Similar to the isolated PB domain, the simulations of the full length model of the ARNO protein reveal that the N-terminal α-helix of the PB domain is more stable than the C-terminus, and again, in agreement with the studies of the isolated domains outlined above, the C-terminus of the phosphorylated ARNO model is more stable. Two salt bridges (phospho-Ser392 makes salt bridges with Lys388 and Lys395) (Figure 12) that were also seen in the isolated form of this peptide stabilize the α-helix at the C-terminus.

In general, the full length model of the ARNO protein with the PB domain with Ser392 in unphosphorylated and phosphorylated states was quite stable during the 200 ns simulation. When the PB domain was in its phosphorylated state, the PH and PB domains were more flexible than the rest of the protein. The rmsd (backbone atoms) of the PH and PB domains of the phosphorylated ARNO protein starts to deviate quite significantly [reaching ~7.5 Å shortly after 20 ns (Figure 13B, red line)] early during the simulation, with the rest of protein staying relatively close to its starting conformation [rmsd of ~2 Å (Figure 13B, black line)]. This large conformational change is associated with domain movements in which the PH domain moves toward the PB domain and the ARNO protein attains a closed conformation, in which the pocket between the Sec7 domain and the PH domain is closed (Figure S8 of the Supporting Information). The so-called closed conformation of ARNO is further stabilized by strong interactions between the PH and PB domain residues. Detailed analyses reveal that phospho-Ser392 from the PB domain strongly interacts with Lys326 from the PH domain through a salt bridge or hydrogen bond (Figure 12). The distance between the side chain atoms of both residues [side chain oxygen atom (OP) of phospho-Ser392 and side chain amino proton of Lys326] is >20 Å at the start of the simulation (Figure 13A, black line). A salt bridge is formed between these residues at ~20 ns, as their separation decreases to <5 Å
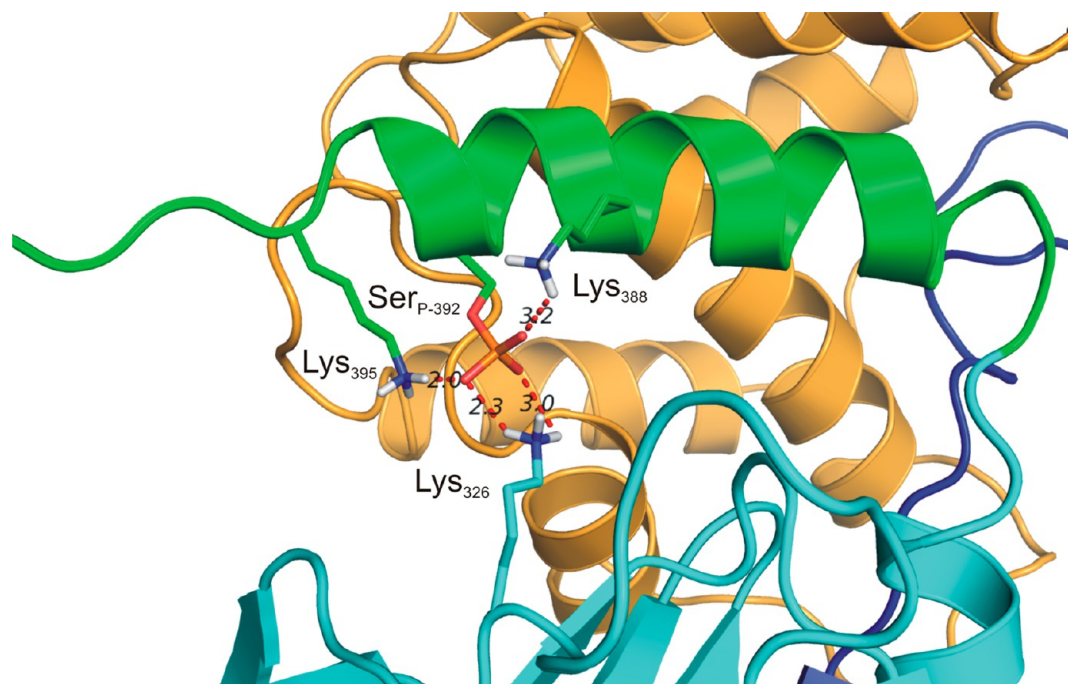

Figure 12. Homology model of the full length ARNO protein without the coiled-coil (CC) domain. Cartoon representation of the Sec7 domain (brown), Sec7-PH linker (LK) domain (blue), PH domain (cyan), and PB domain (green). Structural snapshots illustrating the key residues phospho-Ser392, Lys388, and Lys395 from the PB domain and Lys326 (stick representation) from the PH domain interacting through a salt bridge or hydrogen bond (red dotted lines).
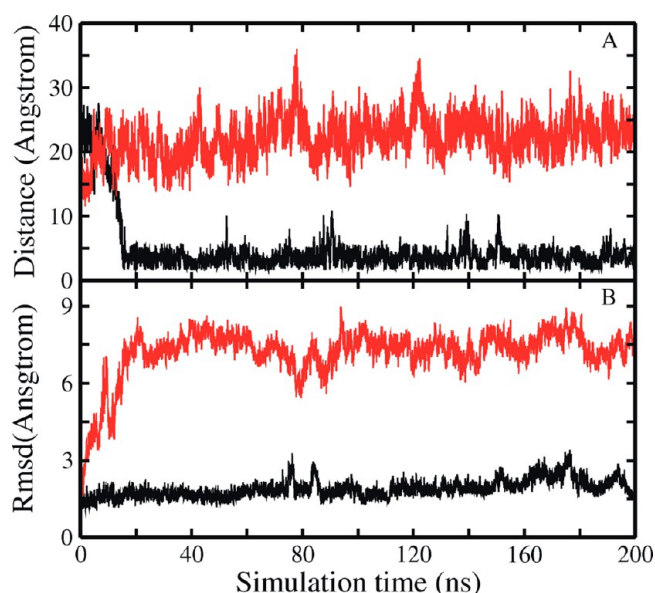
Figure 13. (A) Evolution of a salt bridge during the continuous MD simulation of full length ARNO protein with phosphorylated (black lines) and unphosphorylated (red lines) Ser392. Distance between side chain amino protons of Arg90 and the phospho-Ser392/Ser392 oxygen atoms shown as a function of simulation time. (B) Root-mean-square deviation (backbone atoms) of the sampled conformations [excluding the PB and PH domains (black lines) and for only PH and PB domains (red lines)] of the full length ARNO protein in its phosphorylated Ser392 state in explicit solvent relative to its starting conformation vs simulation time.

(Figure 13A, black line). This interaction is quite stable (distance remains within 5 Å) during the rest of the simulation (Figure 13A, black line). In its unphosphorylated state, this distance remains at ~20 Å (Figure 13A, red lines), as the absence of the phosphate group precludes the formation of analogous salt bridges that serve to bring the two groups together in the phosphorylated state.

These salt bridge interactions increase the stability of the PB domain, and the interdomain interactions induce domain movements, stabilizing the protein in a closed conformation. This reduced conformational flexibility that results from phosphorylation-induced closure likely prevents access to the a2N peptide or protein.

Because the exact interaction sites and/or modes of interaction of the a2N peptide or protein with the ARNO protein are not known, it is not possible to postulate the mechanism of inhibition of interaction upon phosphorylation within the context of the full length protein, as the protein domains are expected to undergo large conformational changes upon binding with a partner protein. Recent studies[7] have found that the N-terminal cytosolic tail of the V-ATPase a2-subunit (a2N) corresponding to its first 17 amino acids modulates the catalytic activity of ARNO via direct interaction with the Sec7 domain by binding at the interaction pocket formed by the catalytic Sec7 and the regulatory PB domain of the ARNO protein. Our simulations of the full length model of ARNO protein with its PB domain phosphorylated and unphosphorylated revealed that, in addition to the increased stability of the PB domain, large conformational changes are induced by the phosphorylation of Ser392 that probably stabilizes the ARNO protein in a closed conformation, i.e., closing the interaction pocket formed by the Sec7, PB, and PH

domains. Thus, our simulation studies provide some hints about the mechanism of inhibition of interaction of ARNO with its partner protein(s), upon phosphorylation.

■ DISCUSSION

Consistent with the experimental studies, our MD simulations reveal significant conformational changes resulting from Ser392 phosphorylation. Simulations predict that the isolated PB domain of the ARNO peptide is highly flexible and undergoes large transitions between collapsed and extended states. During both the MD and BP-REMD simulations, the α-helix at the N-terminus was well-preserved in both phosphorylated and unphosphorylated forms. However, dramatic structural differences were seen for the rest of the peptide. Phosphorylation of Ser392 increases both the helicity and stability at the C-terminus. Upon phosphorylation, the α-helix at the C-terminus is largely conserved with transitions to a 3_{10}-helix. This is associated with the formation of stable salt bridges or hydrogen bonds between phospho-Ser392 and residues Arg390, Lys388, Lys395, and Lys396. These salt bridge interactions increase the stability, particularly in the vicinity of the phosphorylated serine, by constraining the backbone dihedrals of the residues to remain close to α-helical conformations. In contrast, in the absence of phosphorylation, the C-terminus of the peptide is metastable and undergoes rapid structural fluctuations, especially in residues 385−400. The C-terminal α-helix rapidly fluctuates among α-helix, 3_{10}-helix, and turn, while the 3_{10}-helix rapidly unfolds. Simulations also suggest that phosphorylation results in the extension of the α-helix at the N-terminus of the peptide by one turn as a result of stability imparted by a pair of salt bridges between Glu382 and Arg387 and between Glu382 and Lys388. This region does have a propensity to form a helix, as is seen, although infrequently, in simulations of the unphosphorylated state. In summary, simulations demonstrate that phosphorylation of Ser392 induces ordering effects throughout the peptide, resulting in an increase in the overall stability.

Experiments and simulation data for other proteins and peptides have demonstrated unequivocally that both ordering and disordering events accompany phosphorylation. The structural stabilization and destabilization effects of phosphorylation and the associated disorder to order (vice versa) transitions are accompanied by salt bridges and hydrogen bonds, which was also seen in our study. Phosphorylation also increases the stability of the system, particularly in the immediate vicinity of the site of phosphorylation. These findings from the simulations of the isolated PB domain are in good agreement with the recent NMR structures of corresponding ARNO-derived peptides.[7] Our simulations further offer a mechanism that underlies the inhibition of interaction between a2N and the PB domain. It is likely that upon phosphorylation of Ser392, the associated increase in the level of structural ordering and stability of the PB domain together with induced large conformational changes may regulate access to and interactions with a2N. This would result from the increased structural rigidity and the concomitant increase in barriers to transitions to other conformations, which may be needed for stable interactions with other protein partners. In the absence of phosphorylation, the PB domain is metastable, fluctuating between ordered and dynamically disordered conformations so that it can adopt different conformations that interact more strongly with its regulatory partners. Our simulations suggest that the inhibition of site-

specific interactions of the ARNO-derived peptides with a2N is not simply the addition of phosphate groups, but a structural switch that increases the stability coupled to large conformational changes. Thus, the conformational flexibility inferred from our simulations provides a possible explanation of the mechanism of regulation of the catalytic activity of ARNO by PKC-dependent Ser392 phosphorylation.

■ CONCLUSIONS

In this study, we have used MD simulations to investigate the influence of phosphorylation on the C-terminal PB domain of the ARNO protein. In addition to standard MD simulations, BP-REMD simulations were conducted on both phosphorylated and unphosphorylated forms of ARNO-derived peptides, to further enhance the conformational sampling. The simulations suggest that the isolated PB domain of the ARNO protein is highly flexible and the C-terminus is unstable compared to the N-terminus. Our simulation results are in good agreement with complementary experimental data, defining a phosphorylation-induced disorder to order transition, and provide new insight into the structural dynamics of this protein domain. Simulations confirm that in the absence of phosphorylation, the C-terminus of the PB domain is dynamically disordered, undergoing rapid transitions among α-helix, 3_{10}-helix, and turn. Interestingly, the dynamics of structural stability of the corresponding region in the PB domain are highly dependent (regulated or controlled) upon phosphorylation. As seen in the experimental structures, phosphorylation at Ser392 causes a dramatic disorder to order transition in residues 388–396, converting a dynamically unstructured region to a stable α-helix during the simulations. Formation of salt bridges or hydrogen bonds between phospho-Ser392 and Arg390/Lys388, Lys395, and Lys396 is a major contributing factor for the increased stability and helicity of the peptide. This mechanism provides an efficient conformational switch that possibly inhibits the interaction of ARNO with a2N, most likely by imposing structural restrictions on the PB domain (and indeed the whole) of ARNO.

These observations help to explain how the function of ARNO may be regulated by PKC-dependent Ser392 phosphorylation. This study further details this at an atomic level and strengthens the general picture that regulation of dynamic disorder by post-translational modifications is important in biological regulation and energy transduction.

■ ASSOCIATED CONTENT

Ⓢ Supporting Information

Angles between the two α-helices of the sampled ARNO$_{375-400}$ peptide conformations (Figure S1), root-mean-square fluctuations of ARNO$_{375-400}$ peptide conformations (Figure S2), violations of the experimental NOE upper distance bounds (Figure S3), time evolution of the secondary structure of all ARNO$_{375-400}$ peptide simulations (Figure S4), second highly populated structure sampled during BP-REMD of the ARNO$_{375-400}$^{P} peptide (Figure S5), evolution of the salt bridge between Ser392 and Arg390 during MD simulation of the unphosphorylated ARNO$_{375-400}$ peptide (Figure S6), backbone dihedral angle distribution of helix I at the N-termini of both phosphorylated and unphosphorylated ARNO$_{375-400}$ peptides (Figure S7), and structural snapshots showing the superposition of a sampled conformation of the full length ARNO protein model with its starting conformation (Figure S8). This material is available free of charge via the Internet at http://pubs.acs.org.

■ AUTHOR INFORMATION

Corresponding Authors
*Bioinformatics Institute (A*STAR), 30 Biopolis St., 07-01 Matrix, Singapore 138671. E-mail: raghavk@bii.a-star.edu.sg. Telephone: +65 6478 8353. Fax: +65 6478 9048.
*Bioinformatics Institute (A*STAR), 30 Biopolis St., 07-01 Matrix, Singapore 138671. E-mail: chandra@bii.a-star.edu.sg. Telephone: +65 6478 8273. Fax: +65 6478 9048.

Notes
The authors declare no competing financial interest.

■ ACKNOWLEDGMENTS

■ REFERENCES

(1) Casanova, J. E. (2007) Regulation of Arf activation: The Sec7 family of guanine nucleotide exchange factors. *Traffic 8*, 1476–1485.
(2) Bourne, H. R., Sanders, D. A., and McCormick, F. (1990) The GTPase superfamily: A conserved switch for diverse cell functions. *Nature 348*, 125–132.
(3) Donaldson, J. G., and Klausner, R. D. (1994) ARF: A key regulatory switch in membrane traffic and organelle structure. *Curr. Opin. Cell Biol. 6*, 527–532.
(4) D'Souza-Schorey, C., and Chavrier, P. (2006) ARF proteins: Roles in membrane traffic and beyond. *Nat. Rev. Mol. Cell Biol. 7*, 347–358.
(5) Hurtado-Lorenzo, A., Skinner, M., El Annan, J., Futai, M., Sun-Wada, G. H., Bourgoin, S., Casanova, J., Wildeman, A., Bechoua, S., Ausiello, D. A., Brown, D., and Marshansky, V. (2006) V-ATPase interacts with ARNO and Arf6 in early endosomes and regulates the protein degradative pathway. *Nat. Cell Biol. 8*, 124–136.
(6) Marshansky, V. (2007) The V-ATPase a2-subunit as a putative endosomal pH-sensor. *Biochem. Soc. Trans. 35*, 1092–1099.
(7) Hosokawa, H., Dip, P. V., Merkulova, M., Bakulina, A., Zhuang, Z., Khatri, A., Jian, X., Keating, S. M., Bueler, S. A., Rubinstein, J. L., Randazzo, P. A., Ausiello, D. A., Grüber, G., and Marshansky, V. (2013) The N termini of a-subunit isoforms are involved in signaling between vacuolar H⁺-ATPase (V-ATPase) and cytohesin-2. *J. Biol. Chem. 288*, 5896–5913.
(8) Merkulova, M., Bakulina, A., Thaker, Y. R., Grüber, G., and Marshansky, V. (2010) Specific motifs of the V-ATPase a2-subunit isoform interact with catalytic and regulatory domains of ARNO. *Biochim. Biophys. Acta 1797*, 1398–1409.
(9) DiNitto, J. P., Delprato, A., Gabe Lee, M. T., Cronin, T. C., Huang, S., Guilherme, A., Czech, M. P., and Lambright, D. G. (2007) Structural basis and mechanism of autoregulation in 3-phosphoinositide-dependent Grp1 family Arf GTPase exchange factors. *Mol. Cell 28*, 569–583.
(10) Smart, J. L., and McCammon, J. A. (1999) Phosphorylation stabilizes the N-termini of α-helices. *Biopolymers 49*, 225–233.
(11) Espinoza-Fonseca, L. M., Kast, D., and Thomas, D. D. (2007) Molecular dynamics simulations reveal a disorder-to-order transition on phosphorylation of smooth muscle myosin. *Biophys. J. 93*, 2083–2090.
(12) Kast, D., Espinoza-Fonseca, L. M., Yi, C., and Thomas, D. D. (2010) Phosphorylation-induced structural changes in smooth muscle

myosin regulatory light chain. *Proc. Natl. Acad. Sci. U.S.A. 107*, 8207−8212.

(13) Metcalfe, E. E., Traaseth, N. J., and Veglia, G. (2005) Serine 16 phosphorylation induces an order-to-disorder transition in monomeric phospholamban. *Biochemistry 44*, 4386−4396.

(14) Karim, C. B., Zhang, Z., Howard, E. C., Torgersen, K. D., and Thomas, D. D. (2006) Phosphorylation-dependent conformational switch in spin-labeled phospholamban bound to SERCA. *J. Mol. Biol. 358*, 1032−1040.

(15) Paterlini, M. G., and Thomas, D. D. (2005) The α-helical propensity of the cytoplasmic domain of phospholamban: A molecular dynamics simulation of the effect of phosphorylation and mutation. *Biophys. J. 88*, 3243−3251.

(16) Steinmetz, M. O., Jahnke, W., Towbin, H., Garcia-Echeverria, C., Voshol, H., Müller, D., and van Oostrum, J. (2001) Phosphorylation disrupts the central helix in Op18/stathmin and suppresses binding to tubulin. *EMBO Rep. 2*, 505−510.

(17) Missimer, J. H., Steinmetz, M. O., van Gunsteren, W. F., and Dolenc, J. (2012) Influence of 63Ser Phosphorylation and Dephosphorylation on the Structure of the Stathmin Helical Nucleation Sequence: A Molecular Dynamics Study. *Biochemistry 51*, 8455−8463.

(18) Santy, L. C., Frank, S. R., Hatfield, J. C., and Casanova, J. E. (1999) Regulation of ARNO nucleotide exchange by a PH domain electrostatic switch. *Curr. Biol. 9*, 1173−1176.

(19) Kannan, S., and Zacharias, M. (2007) Enhanced sampling of peptide and protein conformations using replica exchange simulations with a peptide backbone biasing-potential. *Proteins 66*, 697−706.

(20) Kannan, S., and Zacharias, M. (2009) Folding of Trp-cage Mini Protein Using Temperature and Biasing Potential Replica Exchange Molecular Dynamics Simulations. *Int. J. Mol. Sci. 10*, 1121−1137.

(21) Kannan, S., and Zacharias, M. (2009) Folding simulations of Trp-cage mini protein in explicit solvent using biasing potential replica-exchange molecular dynamics simulations. *Proteins 76*, 448−460.

(22) Frickenhaus, S., Kannan, S., and Zacharias, M. (2009) Efficient evaluation of sampling quality of molecular dynamics simulations by clustering of dihedral torsion angles and Sammon mapping. *J. Comput. Chem. 30*, 479−492.

(23) Kannan, S., and Zacharias, M. (2010) Application of biasing potential replica exchange simulations for loop modeling and refinement of proteins in explicit solvent. *Proteins 78*, 2809−2819.

(24) Case, D., Pearlman, D. A., Caldwell, J. W., Cheatham, T. E., III, Ross, W. S., Simmerling, C. L., Darden, T. A., Merz, K. M., Stanton, R. V., Cheng, A. L., Vincent, J. J., Crowley, M., Tsui, V., Radmer, R. J., Duan, Y., Pitera, J., Massova, I., Seibel, G. L., Singh, U. C., Weiner, P. K., and Kollman, P. A. (2010) *Amber 9*, University of California, San Francisco.

(25) Jorgensen, W. L., Chandrasekhar, J., Madura, J. D., Impey, R. W., and Klein, M. L. (1983) Comparison of simple potential functions for simulating liquid water. *J. Chem. Phys. 79*, 926−935.

(26) Duan, Y., Wu, A., Chowdhury, C. S., Lee, M. C., Xiong, G., Zhang, W., Yang, R., Cieplak, P., Luo, R., Lee, T., Caldwell, J., Wang, J., and Kollman, P. A. (2003) Pointcharge force field for molecular mechanics simulations of proteins based on condensed-phase quantum mechanical calculations. *J. Comput. Chem. 24*, 1999−2012.

(27) Homeyer, N., Horn, A. H. C., Lanig, H., and Sticht, H. (2006) AMBER force field parameters for phosphorylated amino acids in different protonation states: Phosphoserine, phosphothreonine, phosphotyrosine and phosphohistidine. *J. Mol. Model. 12*, 281−289.

(28) Okamoto, Y. (2004) Generalized-ensemble algorithms: Enhanced sampling techniques for Monte Carlo and molecular dynamics simulations. *J. Mol. Graphics Modell. 22*, 425−439.

(29) Sali, A., and Blundell, T. L. (1993) Comparative protein modelling by satisfaction of spatial restraints. *J. Mol. Biol. 234*, 779−815.

(30) DiNitto, J. P., Delprato, A., Gabe Lee, M. T., Cronin, T. C., Huang, S., Guilherme, A., Czech, M. P., and Lambright, D. G. (2007) Structural basis and mechanism of autoregulation in 3-phosphoinosi-tide-dependent Grp1 family Arf GTPase exchange factors. *Mol. Cell 28*, 569−583.

(31) Darden, T., York, D., and Pedersen, L. (1993) Particle mesh Ewald: An N_log(N) method for Ewald sums in large systems. *J. Chem. Phys. 98*, 10089−10092.

(32) Miyamoto, S., and Kollman, P. A. (1992) Settle: An analytical version of the SHAKE and RATTLE algorithm for rigid water models. *J. Comput. Chem. 13*, 952−962.

(33) Han, B., Liu, Y., Ginzinger, S., and Wishart, D. (2011) SHIFTX2: Significantly improved protein chemical shift prediction. *J. Biomol. NMR 50*, 43−57.

(34) Wishart, D. S., Sykes, B. D., and Richards, F. M. (1992) The Chemical Shift Index: A Fast and Simple Method for the Assignment of Protein Secondary Structure through NMR Spectroscopy. *Biochemistry 31*, 1647−1651.

(35) Feig, M., Karanicolas, J., and Brooks, C. L. (2004) MMTSB tool set: Enhanced sampling and multiscale modeling methods for applications in structural biology. *J. Mol. Graphics Modell. 22*, 377−395.

(36) Humphrey, W., Dalke, A., and Schulten, K. (1996) VMD: Visual molecular dynamics. *J. Mol. Graphics 14*, 33−38.

(37) De Lano, W. (2002) *The PyMOL molecular graphics system*, De Lano Scientific, San Carlos CA.